Thermochimica Acta 481 (2009) 32–45

Contents lists available at ScienceDirect

Thermochimica Acta

journal homepage: www.elsevier.com/locate/tca

Non-isothermal crystallization kinetics of iPP/sPP blends

Louis Garnier, Sophie Duquesne*, Serge Bourbigot, René Delobel

Equipe Procédés d'Elaboration des Revêtements Fonctionnels (PERF), LSPES-UMR/CNRS 8008, Ecole Nationale Supérieure de Chimie de Lille (ENSCL), Avenue Dimitri Mendeleïev-Bât. C7a, BP 90108, 59652 Villeneuve d'Ascq Cedex, France

ARTICLE INFO

Article history:
Received 8 July 2008
Received in revised form
30 September 2008
Accepted 3 October 2008
Available online 17 October 2008

Keywords:
iPP/sPP blend
Differential scanning calorimetry (DSC)
Non-isothermal crystallization kinetics
Macrokinetics models
Effective activation energy

ABSTRACT

Non-isothermal crystallization and subsequent melting behaviour of iPP/sPP blends of various compositions were investigated by differential scanning calorimetry (DSC). Results revealed that sPP crystallizes at a slower rate than iPP. This effect is attenuated when the cooling rate is increased up to 20 °C/min and 25 °C/min. DSC scans showed that stability of primary crystallites of sPP and perfection of iPP crystallites were both increased by decreasing cooling rate. Effective activation energy (ΔE_{X_t}) of sPP, calculated using Friedman iso-conversional method, was found to be lower in iPP/sPP blend than in neat sPP whereas ΔE_{X_t} of iPP is not modified. Results were analysed through Avrami, Ozawa and Mo models. They both showed a decrease of crystal growth dimensionality for both iPP and sPP in iPP/sPP blends compared with neat iPP and sPP. The kinetic parameters U and K_g were determined by the Hoffman–Lauritzen theory.

1. Introduction

Syndiotactic polypropylene (sPP) was first synthesized in the early 1960s with a Ziegler Natta catalyst [1,2]. Unfortunately, this new stereoregular polypropylene presenting very low syndiotacticities had poor mechanical and thermal properties that prevented sPP to have many applications. The use of new metallocene catalysts allowed Ewen et al. to synthesize a sPP with high tacticity in 1988 [3]. This new sPP exhibits interesting properties, such as important toughness and excellent elastic behaviour, and therefore has recently received greater attention and became the centre of many investigations [4–6]. The excellent elastic properties of sPP are based upon a phase transition occurring in crystalline regions during stretching. In fact, four crystalline forms have been found for sPP. In the most stable forms (form I and form II), chains are in a helical conformation whereas they are in a trans-planar conformation in the metastable forms III and IV. Previous investigations have found that stretching of sPP blends and fibers induce a transition from the stable form I or II to form III. The particularity of this transition is its reversible nature because form I or II is obtained again when the applied stress is removed [7–10]. However, besides its excellent elastic properties sPP exhibits many disadvantages such as poor mechanical properties, a very complicated polymorphism and a slow crystallization rate that hinders sPP processing steps like melt spinning [11–14].

Blending sPP with another material having better mechanical properties and a faster crystallization rate can be an alternative for improving processing of sPP and in particular melt spinning [15]. For example, many investigations have been performed on sPP blends with isotactic polypropylene (iPP). Thomman et al. [16] found that iPP/sPP blends are phase separated. They showed that crystallization of iPP and sPP occurs separately and that crystallization of iPP/sPP blend is dependant on the crystallization nature of the neat components. An iPP matrix with dispersed sPP phase or a sPP matrix with iPP dispersed phase can be obtained, depending on the blend composition. Fig. 1 shows transition electron microscopy (TEM) picture of an iPP/sPP blend of composition 75/25. It is observed that iPP constitutes the continuous phase whereas sPP forms nodules.

A co-continuous morphology was also found for nearly symmetric compositions blends [16,17]. Gorassi [15] studied mechanical properties of iPP/sPP fibers and it was shown that blending sPP with iPP improves sPP drawability significantly. Finally, Zhang et al. [11] have investigated morphology and mechanical behaviour of iPP/sPP blends and fibers. It was shown that the addition of sPP induces a decrease of the blend crystallinity and that iPP/sPP fibers exhibit good elastic properties.

Although many investigations have been done on crystallization behaviour and morphology of iPP/sPP blends [11,15–18], no work reports the crystallization kinetics of iPP/sPP blends even

* Corresponding author. Tel.: +33 320 33 72 36; fax: +33 320 43 65 84.
E-mail address: sophie.duquesne@ensc-lille.fr (S. Duquesne).

0040-6031/$ – see front matter © 2008 Elsevier B.V. All rights reserved.
doi:10.1016/j.tca.2008.10.006

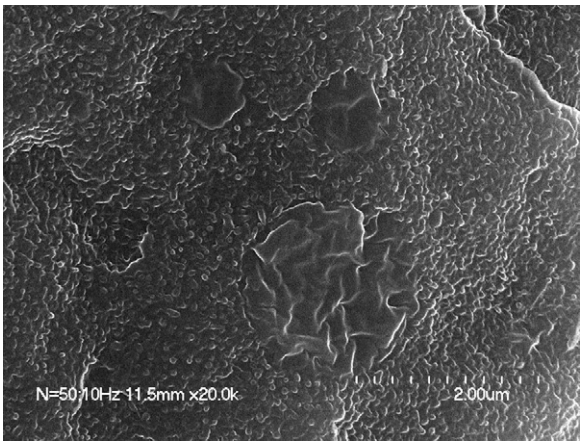

Fig. 1. TEM micrograph of an iPP/sPP blend of composition 75/25.

though crystallization kinetics is an important factor influencing processing steps of semi-crystalline materials.

The aim of this study is to analyse thermal properties and in particular crystallization kinetics of both iPP and sPP in iPP/sPP blends of various compositions. Therefore, iPP/sPP blends of different compositions are prepared and their crystallization kinetics will be investigated through non-isothermal DSC analyses. Results obtained will be analysed focusing three different kinetics models (Avrami, Ozawa and Mo analyses) in order to characterize crystallization mechanisms involved. Determination of the activation energy for both iPP and sPP crystallization in the blends will also be done. Finally, results from the three models will be discussed in the last part of the paper.

2. Experimental

2.1. Materials

Commercial grades of isotactic polypropylene and syndiotactic polypropylene were used in this study. iPP (PPH9069) and sPP (Finaplas 1751) were supplied by Total petrochemicals. PPH9069 has a melt flow index (MFI) of 25 g/min whereas MFI of Finaplas 1751 is 20 g/min.

2.2. Blends preparation

Blends of iPP/sPP (75/25, 50/50, 40/60, 30/70, w/w) were prepared in a Brabender mixer at 190 °C for 12 min with a shear rate of 50 rpm. Homopolymers of iPP and sPP were prepared identically in order to have blends and homopolymers with the same thermal history. Blends were turned into powder prior to thermal analyses using a cryogenic crushing unit.

2.3. Non-isothermal DSC measurements

Non-isothermal crystallization kinetics of iPP/sPP blends were investigated by Differential Scanning Calorimetry using a TA Instruments Q100 Calorimeter. All measurements were performed in nitrogen (nitrogen flow = 50 mL/min) to avoid degradation of the iPP/sPP blend upon heating. 8.3 ± 0.1 mg of each sample were put in a sealed aluminium pan. Samples were first heated up from 25 °C to 200 °C at a rate of 10 °C/min and held for 30 min to erase thermal history of the blend. It appeared to be the lap of time required to erase completely thermal history of a sample and there were no differences with scans performed after holding samples at 200 °C for 5 min. Then samples were cooled down at various cooling rates to 25 °C. The various cooling rates were taken as follows: 1 °C/min, 5 °C/min, 10 °C/min, 15 °C/min, 20 °C/min and 25 °C/min so that six experiments were achieved for each blend. Subsequent melting endotherms were recorded after each experiment at a rate of 10 °C/min.

Table 1
Correspondence between n_A and growth types.

n	Growth type
3–4	Spherulitic-type
2–3	Disc-like
1–2	Fibril-like

Some data could be taken from DSC analysis such as $T_{0.01}$ and $T_{0.99}$ which are temperatures at which degree of crystallinity is 1% and 99% respectively and T_{max} which is the temperature corresponding to the maximal crystallization rate. T_0 (onset temperature of crystallization) was taken as the temperature at which 0.1% of relative crystallinity is achieved. t_{100} which is the time required for both iPP and sPP to achieve 100% crystallinity can also be determined from the DSC data.

3. Theoretical background for crystallization kinetics

From DSC thermogram, the evolution of the relative crystallinity $X_t(T)$ of a component of a blend as a function of temperature can be expressed as:

$$X_t(T) = \frac{\int_{T0}^{T}(dH_C/dT) \times dT}{\Delta H_C} \quad (1)$$

where T_0 and T correspond to the onset temperature of crystallization and to an arbitrary temperature respectively, dH_c/dT represents the variation of the enthalpy of crystallization as a function of temperature variation and ΔH_c is the total enthalpy of crystallization under a specific cooling rate.

If we consider that the difference of temperature between the sample and the DSC furnace is negligible, which was the case in our work, the relationship between time and temperature can be expressed as follows:

$$t = \frac{T_0 - T}{\Phi} \quad (2)$$

where Φ corresponds to the constant cooling rate.

Using Eq. (2) it makes it possible to convert $X_t = f(T)$ curves observed from non-isothermal DSC data into $X_T = f(t)$ curves.

There are many models used to describe the crystallization kinetics of semi-crystalline polymers. In this study three models will be investigated.

First model is the Avrami model in which evolution of relative crystallinity as a function of time is formulated as follows [19–21]:

$$X_T(t) = 1 - \exp(-(K_A \times t)^{n_A}) \in [0, 1] \quad (3)$$

K_A is the crystallization rate constant whereas n_A corresponds to the Avrami coefficient. Both of these constants are specific of nucleation and diffusion type [22]. Table 1 presents the growth type corresponding to each specific value of Avrami coefficient.

Avrami model was first designed for isothermal crystallization but it has been used for the description of nonisothermal crystallization of some semi-crystalline polymers including sPP by using the condition expressed in Eq. (2) [13,22–25].

The second model investigated will be the Ozawa model, which is an extension of the Avrami model based on derivation of Evans [26] to describe non-isothermal crystallization. This is based on the fact that non-isothermal crystallization may be equivalent to a succession of infinitesimal small isothermal crystallization steps

[27]. The main difference compared to the Avrami model is that the time variable is replaced by a cooling rate Φ. In the Ozawa model, the evolution of relative crystallinity of a component of the blend is described by the following Eq. (4) which represents the evolution of relative crystallinity as a function of cooling rate for a given temperature:

$$X_t(T) = 1 - \exp\left(-\left(\frac{K_o}{\Phi}\right)^{n_o}\right) \in [0, 1] \quad (4)$$

where K_o and n_o correspond to the Ozawa crystallization rate constant and the Ozawa coefficient respectively. They have the same meaning as the Avrami parameters [13,27–29].

Finally, the model of Mo will be investigated. This model is based upon the following Eq. (5):

$$\log\Phi = \log F(T) - a \times \log t \quad (5)$$

with $F(T) = (K_O^{n_o}/K_A^{n_A})^{1/n_o}$ and $a = n_A/n_O$. $F(T)$ corresponds to the cooling rate at unit crystallization time when the polymer reaches a certain value of relative cristallinity. Mo model is a combination of both models of Avrami and Ozawa to describe non-isothermal crystallization [23,30–32].

A study of the evolution of the crystallization activation energy as a function of relative crystallinity for both iPP and sPP in the blend was investigated. Kissinger [33] found a very popular treatment and Vyazovkin [34,35] developed an integral iso-conversional method but here, the well known differential iso-conversional Friedman method was chosen because this method is both simple and reliable.

Friedman method is based upon Eq. (6):

$$\ln\left(\frac{dX_t}{dt}\right)_{X_t} = A - \frac{\Delta E_{X_t}}{RT} \quad (6)$$

This can be formulated as:

$$\left(\frac{dX_t}{dt}\right)_{X_t} = \exp\left(A - \frac{\Delta E_{X_t}}{RT}\right) \quad (7)$$

where $(dX_t/dt)X_t$ is the instantaneous crystallization rate for a given relative crystallinity X_t, ΔE_{X_t} is the effective energy barrier for the crystallization process at a given crystallinity and A is a random pre-exponential coefficient [13,36,37]. By calculating values of instantaneous crystallization rate at a given relative crystallinity for various cooling rates, the energy barrier for this specific relative crystallinity can be obtained.

Vyazovkin and Sbirrazzuoli combined Hoffman–Lauritzen theory with isoconversional method and found a temperature dependence of effective activation energy given by the following Eq. (8) [38–40]:

$$\Delta E = U\frac{T^2}{(T - T_\infty)^2} + K_g R\frac{T_m^2 - T_m T - T^2}{(T_m - T)^2 T} \quad (8)$$

U is the activation energy of chain segmental jump, T_m is the equilibrium melting point of the component of the blend (iPP or sPP in our study) whereas T_∞ is the temperature where motion related to the viscous flow is supposed to cease. It is usually taken 30 K below the glass transition T_g which is 271 K for iPP and 283 K for sPP (observed on preliminary DMA measurements). K_g is the nucleation constant and contains contributions from the surface free energies (Eq. (9)).

$$K_g = \frac{n b_0 \delta \delta_e T_m}{k\,\Delta h_f^n} \quad (9)$$

b_o is the width of a monomolecular layer, n is a constant that takes 4 for crystallization regime I and takes 2 for crystallization regime II, δ and δ_e are the lateral and the end surface energies, respectively. k is the Boltzmann constant and ΔH_f is the equilibrium melting enthalpy.

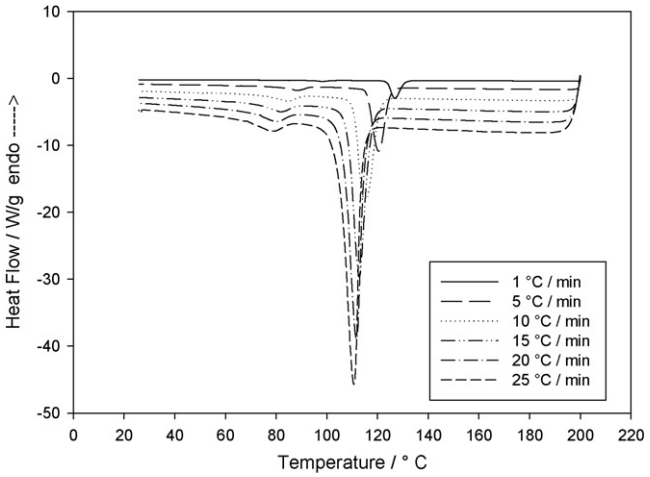

Fig. 2. DSC cooling scans for the 75/25 blend at various cooling rates.

4. Results

4.1. Non-isothermal DSC measurements

Fig. 2 presents crystallization exotherms obtained for the 75/25 blend at different cooling rates, ranked from 1 °C/min to 25 °C/min. A single crystallization peak is observed for each polymer in the blend (iPP and sPP) at each cooling rate. The lower temperature peak (around 80 °C) corresponds to the crystallization of sPP whereas the high temperature peak (around 120 °C) refers to the crystallization of the iPP.

A shift of crystallization temperatures of both iPP and sPP towards lower temperatures is observed when cooling rate increases. Full Width at Half the Maximum (FWHM) for iPP and sPP crystallization exotherms in the 75/25 blends are reported in Table 2.

DSC data and FWHM show that the crystallization exotherm becomes wider for sPP as the cooling rate increases. On the contrary FWHM for iPP is random around the value 5.2 °C.

Moreover, FWHM indicates that the crystallization peak is little bit broader for sPP than for iPP at a specific cooling rate indicating that sPP crystallises little bit slower than iPP does [11]. Subsequent melting endotherms for the 75/25 blend are presented in Fig. 3.

The single high temperature melting endotherm at around 160 °C corresponds to the melting of iPP crystallites and no shift as a function of cooling rate is observed. However, the peak width increases significantly with the cooling rate. As the peak width increases towards lower temperatures, it can be explained by the presence of an increasing number of defects in iPP crystallites due to the increasing cooling rate. On the contrary, the double melting endotherm in the temperature range 110–140 °C belonging to sPP evidences some evolution as a function of the cooling rate. The lower temperature melting endotherm size increases by decreasing the cooling rate whereas size and sharpness of the second melting

Table 2
FWHM for both iPP and sPP crystallization peaks in the 75/25 blend.

Φ (°C/min)	FWHM for iPP (°C)	FWMH for sPP (°C)
1	4	5.2
5	5.3	6.9
10	6.3	8.8
15	5.2	8.9
20	4.9	9.7
25	5.2	10.7

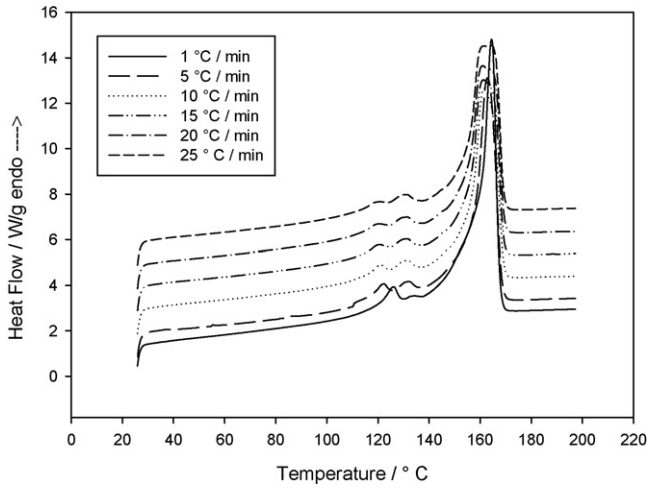

Fig. 3. DSC heating scans for the 75/25 blend.

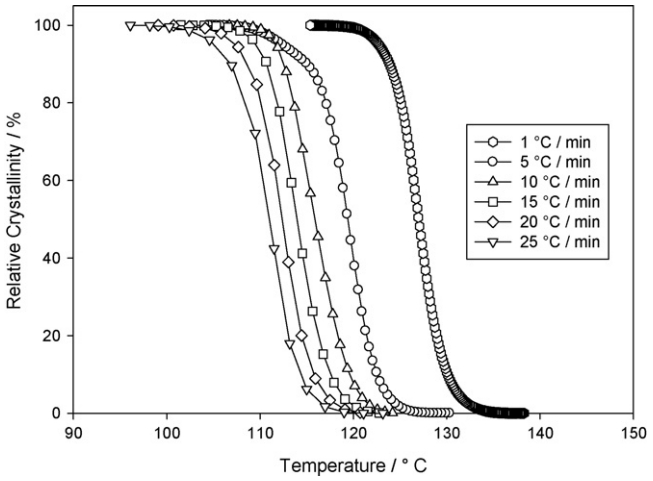

Fig. 4. $X_t = f(T)$ curves for iPP in 50/50 as a function of cooling rate.

Table 3
Subsequent T_m (°C) for iPP in neat iPP and in 75/25, 50/50, 40/60 and 30/70 blends as a function of cooling rate.

Φ (°C/min)	T_m (°C)				
	Neat iPP	75/25	50/50	40/60	30/70
1	164.4	164.1	164.3	164.4	164.2
5	165.0	163.2	162.6	162.0	161.4
10	163.5	161.4	161.7	161.1	160.8
15	161.4	161.1	160.8	161.7	160.8
20	160.8	160.8	160.8	162.3	161.4
25	160.5	162.3	163.8	161.7	161.7

endotherm remains almost unchanged excepted when the cooling rate is low (1 °C/min) where the peak disappears almost completely. Moreover, the lower temperature melting endotherm is shifted towards higher temperatures by decreasing cooling rate. In fact, the first melting endotherm is associated with partial melting of less stable fraction of primary crystallites in disordered forms I or II and their recrystallization in more ordered form I or II. Then, the higher temperature melting endotherm corresponds to the remelting of the recrystallized crystallites in addition with the melting of the more stable fraction of primary crystallites already in more ordered form I or II [9,41,42]. Consequently the shift of the sPP first melting endotherm towards higher temperatures are consistent with the work done by Supaphol et al. [13,43] which indicates an improvement of the stability of primary crystallites of sPP with decreasing cooling rate. The other blends, as well as neat polymers, present a similar DSC thermal behaviour. Subsequent melting temperatures for iPP and sPP in the different blends investigated are presented in Tables 3 and 4, respectively. T_{m1} and T_{m2} refer to the lower temperature melting endotherm and the higher temperature melting endotherm for sPP respectively.

Table 4
Subsequent T_{m1} and T_{m2} (°C) for sPP in neat sPP and in 75/25, 50/50, 40/60 and 30/70 blends as a function of cooling rate.

Φ (°C/min)	T_{m1}/T_{m2} (°C)				
	Neat sPP	75/25	50/50	40/60	30/70
1	124.9/132.7	125.9/133.3	122.6/130.9	126.6/133.8	127.3/133.3
5	118.8/130.9	122.3/131.8	124.1/131.5	122.9/131.5	123.2/131.5
10	116.1/130.3	121.1/130.6	122.9/131.8	122.6/131.2	122.6/131.5
15	111.1/129.4	120.5/130.6	120.5/130.3	121.7/130.9	121.1/130.6
20	109.9/130.0	119.4/130.9	119.1/129.8	120.8/130.3	120.5/130.6
25	109.9/129.7	130.5/129.4	118.0/129.8	119.6/130.0	119.9/130.6

A shift of first melting endotherm T_{m1} towards higher temperatures by decreasing cooling rate is observed in neat sPP and in iPP/sPP blends.

From the DSC data, the variation of the relative crystallinity as a function of temperature for both iPP and sPP in the iPP/sPP blends could be obtained. As an example, Figs. 4 and 5 show the variation of the relative crystallinity X_t as a function of temperature for iPP and sPP in the 50/50 blend respectively.

As it has been mentioned above with DSC scans, the temperature range in which crystallization occurs is shifted towards lower temperatures as the cooling rate increases for both iPP and sPP. A decrease of the slope of the $X_t = f(T)$ curves is also observed as the cooling rate increases. This effect is more pronounced for sPP. Similar curves were observed for all materials including neat iPP and sPP. $T_{0.01}$, $T_{0.99}$ and T_{max} for both iPP and sPP were determined from the $X_t(T)$ curves (Tables 5 and 6 report the values obtained for both iPP and sPP in all blends, respectively).

It can be observed that for a given blend, $T_{0.01}$, $T_{0.99}$ and T_{max} decrease when the cooling rate increases (this observation has been made above in Figs. 4 and 5 about 50/50 blend). However, blend composition seems to have no particular effect on $T_{0.01}$, $T_{0.99}$ and T_{max} except for neat sPP where $T_{0.01}$ and $T_{0.99}$ values are a bit lower than in iPP/sPP blends.

As it was mentioned earlier, $X_t(T)$ curves can be converted into $X_T(t)$ curves using Eq. (2). The $X_T(t)$ curves for both iPP

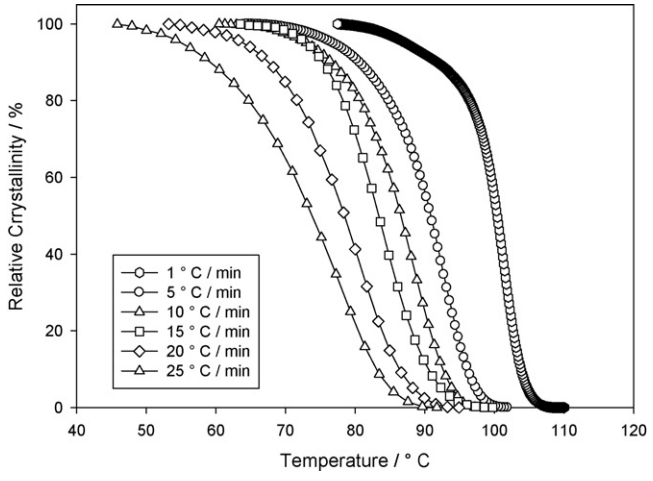

Fig. 5. $X_t = f(T)$ curves for sPP in 50/50 blend as a function of cooling rate.

Table 5
$T_{0.01}$, $T_{0.99}$ and T_{max} for iPP in neat iPP and in 75/25, 50/50, 40/60 and 30/70 blends as a function of cooling rate.

Φ (°C/min)	Neat iPP			75/25			50/50		
	$T_{0.01}$ (°C)	$T_{0.99}$ (°C)	T_{max} (°C)	$T_{0.01}$ (°C)	$T_{0.99}$ (°C)	T_{max} (°C)	$T_{0.01}$ (°C)	$T_{0.99}$ (°C)	T_{max} (°C)
1	134.5	119.7	127.1	134.1	121.8	126.7	135.7	120.5	126.7
5	128.7	109.2	121.1	128	112.3	120.7	128	107.5	119.4
10	125.3	105.9	116.3	124.5	106.9	115.2	124.1	110	115.1
15	123.3	97.4	113.4	121.9	104	112.8	122.6	107.3	113.2
20	121.5	97.1	112.2	119.9	101.2	111.7	119.1	104.6	112
25	119.5	95.5	111.1	118.4	98.8	110.7	117.6	101.8	110.9

Φ (°C/min)	40/60			30/70		
	$T_{0.01}$ (°C)	$T_{0.99}$ (°C)	T_{max} (°C)	$T_{0.01}$ (°C)	$T_{0.99}$ (°C)	T_{max} (°C)
1	136.7	120.8	128.5	135.3	120.2	127.1
5	130.5	109.4	120.9	129.1	109.1	120
10	126.9	102.9	116.9	124.9	101.8	116.3
15	124.9	99.3	113.9	123.5	98.9	114
20	123.7	99.3	112.4	121.3	98.5	112.1
25	122.7	100.9	111.1	117.9	102.4	110

Table 6
$T_{0.01}$, $T_{0.99}$ and T_{max} for sPP in neat sPP and in 75/25, 50/50, 40/60 and 30/70 blends as a function of cooling rate.

Φ (°C/min)	Neat sPP			75/25			50/50		
	$T_{0.01}$ (°C)	$T_{0.99}$ (°C)	T_{max} (°C)	$T_{0.01}$ (°C)	$T_{0.99}$ (°C)	T_{max} (°C)	$T_{0.01}$ (°C)	$T_{0.99}$ (°C)	T_{maz} (°C)
1	105.9	84.9	98.8	104.7	89.8	98.1	107.9	81.7	101.2
5	94.1	68.5	92.2	95.4	73.6	88.1	101.3	72.6	92.3
10	87.6	60.3	87.8	91.9	64.8	84.3	96.2	67.3	88.4
15	83.7	55.4	84.1	88.2	68.9	81.7	98.3	68.8	83.3
20	81.1	51.7	82.1	88.6	65.1	79.8	93.6	56.6	80.2
25	78.8	47.4	81.1	86.3	65.1	78.7	90.3	48.6	76.8

Φ (°C/min)	40/60			30/70		
	$T_{0.01}$ (°C)	$T_{0.99}$ (°C)	T_{max} (°C)	$T_{0.01}$ (°C)	$T_{0.99}$ (°C)	T_{max} (°C)
1	108.5	91.8	101.4	108.1	82.2	98.4
5	101.4	73.9	92.2	101.3	74.6	92.4
10	96.6	70.5	87.8	96.4	72.8	88.1
15	92.8	69.8	84.1	93.2	70.7	85.1
20	91.5	67.8	82.1	91.4	68.8	82.6
25	91.3	59.8	81.1	92.4	65.3	80.5

and sPP in 50/50 blend are presented in Figs. 6 and 7 respectively.

Each curve presents a similar sigmoidal shape which consists of a linear trend between 20% and 80% of relative crystallinity. The trend tends to level off between 0% and 20% and it corresponds to an induction period. The trend also levels off after 80% of relative crystallinity, due to the occurrence of a secondary crystallization process which is due to slower crystallization and perfection of crystals in the later stages [44].

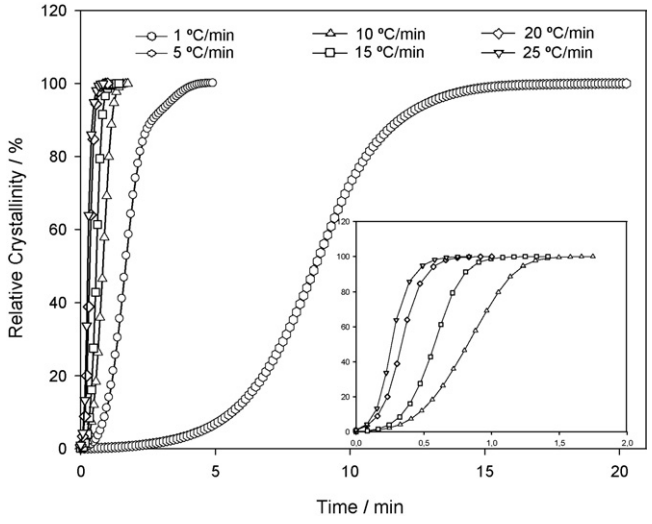

Fig. 6. $X_T = f(t)$ curves for iPP in 50/50 blend as a function of cooling rate.

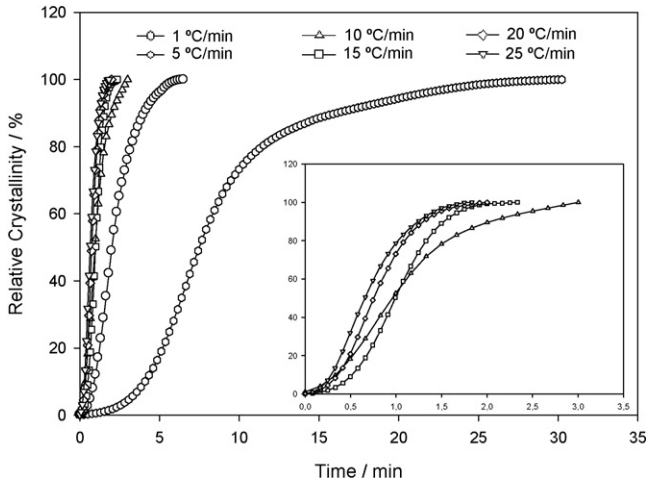

Fig. 7. $X_T = f(t)$ curves for sPP in 50/50 blend as a function of cooling rate.

Table 7
t_{100} values for iPP in neat iPP and in 75/25, 50/50, 40/60 and 30/70 blends as a function of cooling rate.

Φ (°C/min)	t_{100} (min)				
	Neat iPP	75/25	50/50	40/60	30/70
1	31.2	19.9	19.3	19.8	18.6
5	6.0	4.6	4.9	5.1	4.8
10	2.9	2.8	1.8	2.8	2.8
15	2.4	1.8	1.4	1.9	1.9
20	1.9	1.4	1.0	1.5	1.4
25	1.6	1.1	0.9	1.2	0.8

It can be clearly seen that for low cooling rates (1–10 °C/min) the time required for sPP to crystallize is longer than that required for iPP. sPP has therefore a lower crystallization rate than iPP as it has been already suggested by larger crystallization exotherms for sPP. However the difference between crystallization rates of iPP and sPP seems to be attenuated as the cooling rate is increased. It could be useful information if iPP/sPP blends processing is considered. Similar data was found for the other blends. Tables 7 and 8 present t_{100} for iPP and sPP in the various blends investigated and at the different cooling rates respectively.

There is a decrease of t_{100} as the cooling rate increases for both iPP and sPP in all materials. As observed in Figs. 6 and 7, t_{100} taken for a specific blend at a defined cooling rate is generally longer for sPP than for iPP. It is particularly true for low cooling rates. However, while the cooling rate increases, the difference between t_{100} for iPP and sPP decreases and for the highest values of cooling rate (20 °C/min and 25 °C/min) t_{100} for sPP is slightly lower or almost equal to that for iPP. sPP crystallization rate seems to increase faster with the cooling rate than iPP crystallization rate does. Moreover, it can be seen that for a specific cooling rate t_{100} for iPP and sPP are higher in neat materials than in iPP/sPP blends. Finally, it is noteworthy that for each cooling rate the lowest t_{100} values for sPP are in the 75/25 blend. Actually sPP is in the dispersed phase in the 75/25 blend.

4.2. Avrami analysis

Using non-linear fitting procedure of the data for different cooling rates like those presented in Figs. 6 and 7 with Eq. (3) the different parameters n_A, K_A and r^2 can be calculated. Figs. 8 and 9 present $X_T = f(t)$ curves of iPP and sPP in 50/50 blend, respectively. Solid lines represent fits of Eq. (3).

Results obtained for both iPP and sPP in the various blends are presented in Tables 9 and 10 respectively.

n_A values lay mainly between 2 and 3 for sPP in all materials whatever the cooling rate which indicates that disc-like growth is the predominant mechanism taking place in sPP crystallization. For iPP n_A values lie between 3 and 4 in neat iPP and in 75/25 and 50/50 blend whatever the cooling rate. This suggests that iPP crystallizes randomly with a spherulitic growth type in these blends, as in neat

Table 8
t_{100} values for sPP in neat sPP and in 75/25, 50/50, 40/60 and 30/70 blends as a function of cooling rate.

Φ (°C/min)	t_{100} (min)				
	75/25	50/50	40/60	30/70	Neat sPP
1	18.4	26.3	19.4	25.5	36.8
5	4.8	6.6	6.5	6.2	6.4
10	2.7	3.0	3.3	2.8	3.4
15	1.4	2.3	1.8	1.8	2.3
20	1.3	2.0	1.5	1.4	1.7
25	0.9	1.8	1.3	1.3	1.5

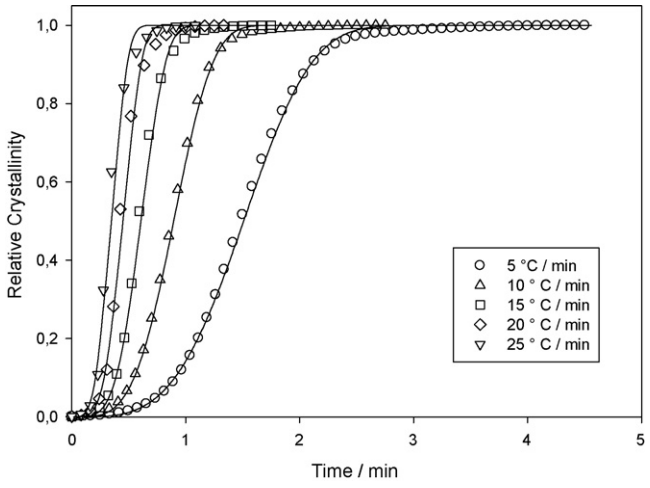

Fig. 8. $X_T = f(t)$ curves for iPP in 50/50 blend as a function of cooling rate with solid lines as fits of Eq. (3).

iPP. However, n_A values decrease in 40/60 and 30/70 blends and lie between 2.4 and 3.4. In these blends, iPP is the dispersed phase so it should be submitted to more stress and therefore a part of iPP should be forced to crystallize in only two directions instead of three. K_A increases with the cooling rate for both iPP and sPP which is expected since the crystallization rate increases with the cooling rate according to Fig. 3. It is noteworthy that the blend composition has no particular effect on K_A, but however, neat iPP and sPP exhibit lower K_A values than the iPP/sPP blends. It indicates, according to Avrami's model, that crystallization rate is lower in neat iPP and sPP compared to crystallization rate in iPP/sPP blends. Fitting coefficient (r^2) lies between 0.979 and 0.999 which shows a good fit between Avrami model and the experimental data. The high values of F_{stat} coefficients confirm the statistical reliability of the results.

4.3. Ozawa analysis

By fitting the data from $X_t(T)$ curves such as these presented in Figs. 4 and 5 for different temperatures taken in the crystallization range with Eq. (4) n_O and K_O values can be calculated. Figs. 10 and 11 present the efficiency of fitting for iPP and sPP in 40/60 blend, respectively.

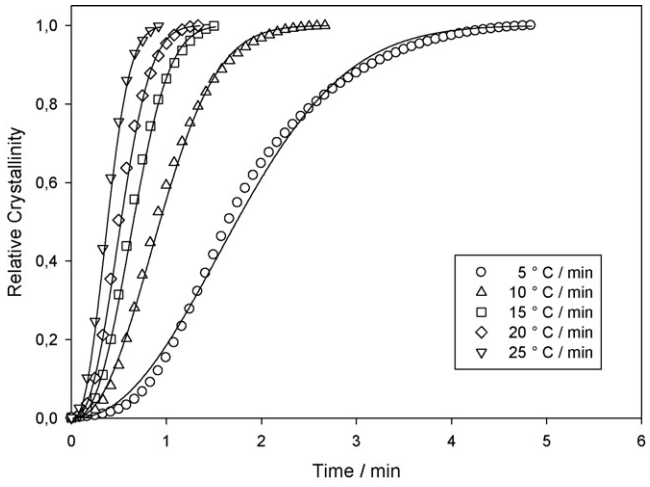

Fig. 9. $X_T = f(t)$ curves for sPP in 50/50 blend as a function of cooling rate with solid lines as fits of Eq. (3).

Table 9
Non-isothermal crystallization kinetics of iPP for neat iPP and for iPP/sPP blends based on Avrami model.

Φ (°C/min)	Neat iPP				75/25				50/50			
	K_A (min^{-1})	n_A	r^2	F_{stat}	K_A (min^{-1})	n_A	r^2	F_{stat}	K_A (min^{-1})	n_A	r^2	F_{stat}
1	0.129	4.22	0.999	2939056	1.034	3.82	0.999	2145687	0.104	4.16	0.999	2303575
5	0.596	3.58	0.998	498223	0.608	3.70	0.999	146528	0.522	2.90	0.995	141376
10	1.017	3.65	0.999	417281	1.052	3.96	0.998	429630	1.095	3.35	0.999	754076
15	1.402	3.76	0.997	137800	1.553	4.23	0.995	11530	1.571	3.73	0.999	630250
20	1.905	3.65	0.996	68684	2.118	4.02	0.979	1946	2.621	2.87	0.999	128298
25	2.542	3.28	0.994	37746	2.743	3.44	0.968	1045	3.293	2.71	0.998	62581

Φ (°C/min)	40/60				30/70			
	K_A (min^{-1})	n_A	r^2	F_{stat}	K_A (min^{-1})	n_A	r^2	F_{stat}
1	0.108	3.39	0.998	125601	0.109	3.34	0.998	1240619
5	0.465	2.83	0.995	144115	0.498	2.51	0.995	104846
10	0.882	2.80	0.994	59145	0.971	2.39	0.992	39929
15	1.265	2.79	0.997	77342	1.407	2.92	0.994	37704
20	1.683	2.93	0.998	125852	1.980	3.08	0.998	77924
25	2.086	3.06	0.998	85080	2.901	2.86	0.999	141004

Table 10
Non-isothermal crystallization kinetics of sPP for neat sPP and for iPP/sPP blends based on Avrami model.

Φ (°C/min)	Neat sPP				75/25				50/50			
	K_A (min^{-1})	n_A	r^2	F_{stat}	K_A (min^{-1})	n_A	r^2	F_{stat}	K_A (min^{-1})	n_A	r^2	F_{stat}
1	0.089	3.11	0.999	5650250	0.131	2.97	0.998	282297	0.106	2.06	0.988	199297
5	0.371	2.95	0.999	2200396	0.495	2.17	0.991	30018	0.396	1.93	0.997	342346
10	0.683	2.67	0.999	1008061	0.932	2.22	0.995	31796	0.833	1.71	0.998	239138
15	0.946	2.53	0.997	919069	1.361	2.45	0.997	31950	0.883	2.87	0.999	2320190
20	1.184	2.49	0.999	604297	1.704	2.37	0.997	25145	1.116	2.34	0.999	506328
25	1.366	2.50	0.999	395727	2.337	2.27	0.999	120653	1.247	2.02	0.999	340267

Φ (°C/min)	40/60				30/70			
	K_A (min^{-1})	n_A	r^2	F_{stat}	K_A (min^{-1})	n_A	r^2	F_{stat}
1	0.137	2.19	0.996	207710	0.109	2.24	0.988	244511
5	0.411	2.70	0.998	1207668	0.423	2.17	0.996	188599
10	0.876	2.06	0.999	480155	0.923	2.12	0.999	156159
15	1.363	2.13	0.999	894016	1.427	2.14	0.999	494551
20	1.658	2.42	0.999	472903	1.776	2.26	0.999	486204
25	1.896	2.44	0.999	321400	1.702	2.69	0.999	288675

Results for both iPP and sPP are presented in Tables 11 and 12 respectively.

n_O exhibits the same evolution as above for n_A and therefore very similar conclusions can be drawn. In the 75/25 blend and in neat iPP, n_O lie between 3 and 4 which indicates that iPP crystallizes with a spherulitic growth type. However, n_O values are lower in the 50/50 considering n_O which lies between 2 and 3. Therefore, some disc-like growth combined with a spherulitic-like crystal growth should

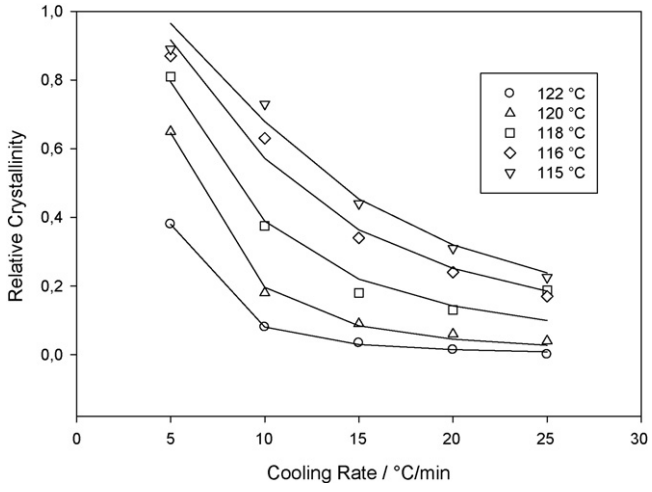

Fig. 10. Relative crystallinity as a function of cooling rate for iPP with solid lines as fits of Eq. (4).

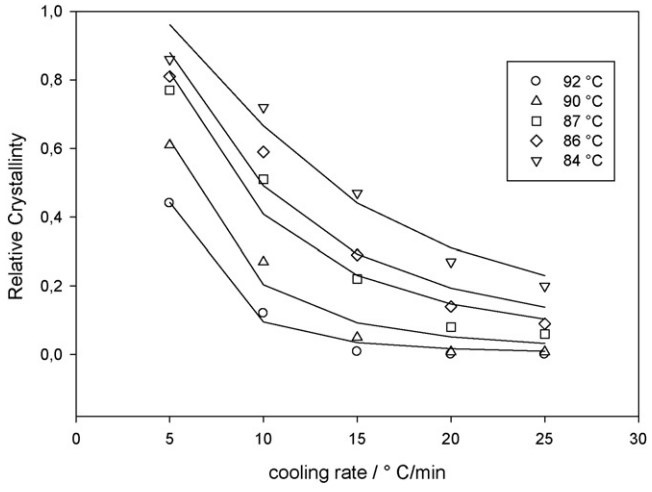

Fig. 11. Relative crystallinity as a function of cooling rate for sPP with solid lines as fits of Eq. (4).

Table 11
Non-isothermal crystallization kinetics of iPP for neat material and for iPP/sPP blends based on Ozawa model.

Neat iPP					75/25					50/50				
T (° C)	K_o (min^{-1})	n_o	r^2	F_{stat}	T (°C)	K_o (min^{-1})	n_o	r^2	F_{stat}	T (°C)	K_o (min^{-1})	n_o	r^2	F_{stat}
117	8.626	4.03	0.996	947	117	7.051	3.12	0.995	594	117	6.364	2.18	0.991	319
116	9.451	3.45	0.996	1089	116	8.888	4.15	0.997	1363	116	7.322	2.19	0.976	120
115	10.677	3.19	0.997	1364	115	9.835	3.69	0.998	1894	115	9.821	2.35	0.969	94
114	12.220	2.83	0.994	731	114	11.126	3.22	0.991	709	114	11.89	2.35	0.968	90
113	14.213	2.43	0.994	654	113	13.241	3.65	0.993	692	113	13.954	2.02	0.946	52

40/60					30/70				
T (°C)	K_o (min^{-1})	n_o	r^2	F_{stat}	T (°C)	K_o (min^{-1})	n_o	r^2	F_{stat}
122	3.727	2.51	0.999	3777	117	7.065	1.65	0.867	20
120	5.086	2.25	0.998	1110	116	8.32	1.62	0.861	18
118	6.565	1.68	0.968	91	115	10.911	2.04	0.868	19
116	8.984	1.55	0.981	155	114	12.696	2.17	0.894	25
115	10.856	1.56	0.973	107	113	13.899	2.04	0.931	40

Table 12
Non-isothermal crystallization kinetics of sPP for neat material and for iPP/sPP blends based on Ozawa model.

Neat sPP					75/25					50/50				
T (° C)	K_o (min^{-1})	n_o	r^2	F_{stat}	T (°C)	K_o (min^{-1})	n_o	r^2	F_{stat}	T (°C)	K_o (min^{-1})	n_o	r^2	F_{stat}
74	9.560	2.97	0.994	540	85	5.405	1.96	0.984	182	90	4.755	1.87	0.976	123
72	10.932	2.61	0.995	632	83	7.059	1.59	0.966	88	88	5.820	1.69	0.951	58
71	11.737	2.47	0.995	660	82	8.267	1.47	0.963	78	86	7.260	1.60	0.921	35
70	12.642	2.35	0.995	640	81	9.758	1.39	0.959	71	85	8.226	1.61	0.911	31
69	13.635	2.25	0.995	641	80	11.69	1.29	0.958	69	84	9.949	1.86	0.904	28

40/60					30/70				
T (° C)	K_o (min^{-1})	n_o	r^2	F_{stat}	T (°C)	K_o (min^{-1})	n_o	r^2	F_{stat}
92	4.052	2.54	0.967	87	90	5.126	2.11	0.976	70
90	4.952	2.1	0.948	54	89	5.703	1.93	0.969	48
87	6.873	1.71	0.949	55	88	6.394	1.79	0.959	54
86	7.887	1.65	0.983	245	87	7.267	1.69	0.947	92
84	10.611	1.56	0.947	54	86	8.446	1.63	0.940	126

be observed in this blend. Finally, n_O decreases between 1.6 and 2.5 in 40/60 and 30/70 blends suggesting that some parts of iPP crystallize in fibrils due to increasing stress. Neat sPP presents n_O values comprised between 2 and 3 whereas in the blends n_O lies between 1 and 2. This indicates that according to Ozawa model neat sPP crystallizes with a disc like growth whereas the main growth type taking place for sPP crystallization in iPP/sPP blends is fibril like. K_O increases with the temperature which was expected because crystallization rate increases with supercooling. However, although Avrami and Ozawa analyses exhibit similar evolutions for n_O and n_A, there are still some differences compared to Avrami analysis. The blend composition has no effect on K_O. However, neat iPP and sPP exhibit higher K_O values compared with K_O values for iPP/sPP blends. It indicates that, according to Ozawa's model, crystallization rate is higher in neat iPP and sPP than in iPP/sPP blend. Fitting coefficient r^2 values lie between 0.861 and 0.999 which indicates a good fit of experimental data with Ozawa model even if r^2 parameter values are a bit lower for Ozawa model than for Avrami model. However, F_{stat} coefficients are significantly lower than those calculated with Avrami analysis suggesting the better accuracy of the Avrami method.

4.4. Mo analysis

By fitting the data from $X_T(t)$ curve in Figs. 6 and 7 in Eq. (5) for various values of relative crystallinity, a and $F(T)$ can be calculated. Figs. 12 and 13 present the efficiency of fitting for iPP and sPP in 30/70 blend, respectively.

The results for Mo's analysis model are presented in the Tables 13 and 14 respectively.

Values of $F(T)$ increase with the relative crystallinity which makes sense because according to the meaning of $F(T)$, it means that at a unit crystallization time a higher cooling rate should be used to increase the relative crystallinity. a values remain relatively constant as the degree of crystallinity increases for each blends, indicating that the ratio between n_A and n_O remains constant what-

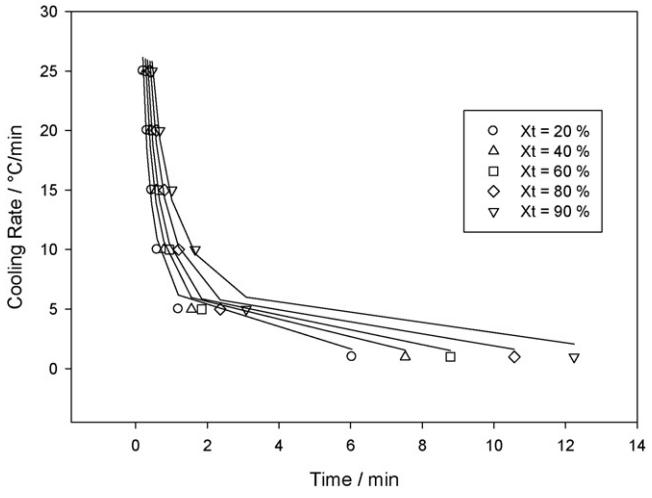

Fig. 12. Cooling rate as a function of time for iPP with solid lines as fits of Eq. (5).

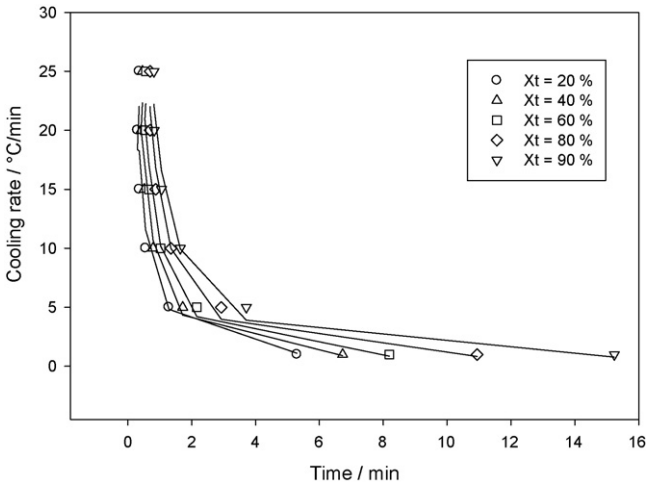

Fig. 13. Cooling rate as a function of time for sPP with solid lines as fits of Eq. (5).

ever the relative crystallinity. *a* parameter is almost close to 1 for all the blends and it is an indication that predictions of nucleation and growth mechanisms according to Avrami and Ozawa are not very different. Nevertheless, the slight deviations from 1 suggest that slight differences still remain between Avrami and Ozawa predictions as it has been observed above. The Mo analysis showed a relatively good agreement with experimental data according to the high values of r^2 for both iPP and sPP. However, F_{stat} coefficients are significantly lower than those calculated with Avrami analysis suggesting the better accuracy of the Avrami method as in the case of Ozawa analysis.

4.5. Activation energy of iPP/sPP blends crystallization

The values of the activation energy as a function of relative crystallinity for both iPP and sPP in the blends according to Friedman method and the corresponding r^2 fit coefficients are presented in Tables 15 and 16 respectively.

It is observed that the values of ΔE_{X_t} are lower for iPP than for sPP. This shows that a lower energy barrier has to be overcome for crystallization of iPP than for crystallization of sPP. Consequently crystallization of iPP is more promoted than crystallization of sPP according to thermodynamic considerations. Figs. 14 and 15 present the evolutions of ΔE_{X_t} for both iPP and sPP in the different materials as a function of relative crystallinity respectively.

The effective activation energy for iPP crystallization presents different evolutions depending on the blend composition. In neat iPP as well as in 75/25 and 50/50 blends, ΔE_{X_t} of iPP increases slowly whereas in 40/60 and 30/70 blends where iPP is in the dispersed phase ΔE_{X_t} remains almost constant until 80% of relative crystallinity. Beyond 80% of relative crystallinity ΔE_{X_t} starts decreasing very rapidly. It is noteworthy that, between 20% and 80% of relative crystallinity, ΔE_{X_t} values are not so different from one blend composition to another. For each blend composition ΔE_{X_t} of sPP remains almost constant during the increase of relative crystallinity. However, the average value differs from one blend composition to another. Neat sPP presents the highest values fol-

Table 13
Non-isothermal crystallization kinetics of iPP for neat material and for iPP/sPP blends based on Mo model.

$X(t)$ (%)	Neat iPP				75/25				50/50			
	a	$F(T)$	r^2	F_{stat}	a	$F(T)$	r^2	F_{stat}	a	$F(T)$	r^2	F_{stat}
20	0.98	6.986	0.988	344	0.99	6.654	0.993	590	1.34	6.876	0.867	25
40	0.95	8.437	0.988	347	0.94	8.091	0.994	636	1.50	10.445	0.938	60
60	0.98	9.653	0.991	473	0.94	9.193	0.995	941	1.67	15.371	0.970	131
80	1.04	11.421	0.994	777	1.01	1.625	0.998	2464	1.76	24.680	0.980	198
90	1.12	13.28	0.997	1498	1.11	1.108	0.999	10342	1.78	32.450	0.991	452

$X(t)$ (%)	40/60				30/70			
	a	$F(T)$	r^2	F_{stat}	a	$F(T)$	r^2	F_{stat}
20	1.05	6.841	0.999	239795	0.82	7.158	0.980	194
40	1.1	8.993	0.999	103514	0.84	8.695	0.986	275
60	1.09	10.897	0.999	19628	0.86	9.982	0.989	362
80	1.07	13.233	0.999	18987	0.84	11.931	0.992	501
90	0.95	15.834	0.998	3267	0.77	14.278	0.990	390

Table 14
Non-isothermal crystallization kinetics of sPP for neat material and for iPP/sPP blends based on Mo model.

$X(t)$ (%)	Neat sPP				75/25				50/50			
	a	$F(T)$	r^2	F_{stat}	a	$F(T)$	r^2	F_{stat}	a	$F(T)$	r^2	F_{stat}
20	1.19	8.223	0.997	1849	1.09	5.668	0.998	3343	0.76	6.802	0.986	282
40	1.26	11.647	0.997	1447	0.99	8.199	0.991	487	0.78	8.170	0.989	370
60	1.32	15.643	0.997	1331	1.02	10.332	0.994	700	0.79	9.247	0.992	472
80	1.33	21.299	0.999	3667	1.00	13.575	0.995	822	0.84	10.499	0.994	747
90	1.29	25.101	0.999	7966	0.97	16.261	0.992	522	0.87	11.658	0.996	977

$X(t)$ (%)	40/60				30/70			
	a	$F(T)$	r^2	F_{stat}	a	$F(T)$	r^2	F_{stat}
20	1.28	4.85	0.975	153	1.04	6.255	0.852	23
40	1.23	7.703	0.986	289	1.15	8.097	0.910	40
60	1.19	10.537	0.991	462	1.19	10.498	0.935	58
80	1.14	14.443	0.992	499	1.19	14.240	0.954	84
90	1.11	17.388	0.981	207	1.15	17.594	0.964	107

Table 15
Effective energy barrier for non-isothermal crystallization of iPP for neat material and for iPP/sPP blends according to the differential iso-conversional method of Friedman.

$X(T)$ (%)	Neat iPP			75/25			50/50		
	ΔE_{X_t} (kJ/mol)	A	r^2	ΔE_{X_t} (kJ/mol)	A	r^2	ΔE_{X_t} (kJ/mol)	A	r^2
10	−17.052	−13.107	0.993	−18.485	−14.683	0.986	−18.130	−14.209	0.991
20	−17.692	−13.043	0.989	−19.613	−15.496	0.989	−19.750	−15.578	0.998
30	−17.409	−13.017	0.990	−19.788	−15.550	0.986	−21.334	−17.115	0.999
40	−16.967	−12.532	0.992	−18.952	−14.630	0.993	−21.827	−17.618	0.999
50	−16.326	−11.913	0.993	−18.366	−14.045	0.993	−21.535	−17.366	0.995
60	−15.377	−11.034	0.994	−17.079	−12.790	0.992	−20.350	−16.229	0.987
70	−14.023.	−9.810	0.994	−14.820	−10.588	0.986	−18.898	−14.885	0.972
80	−13.379	−9.487	0.989	−11.492	−7.399	0.955	−16.285	−12.455	0.924
90	−8.448	−5.074	0.908	−8.101	−4.533	0.894	−13.276	−10.016	0.943

$X(T)$ (%)	40/60			30/70		
	ΔE_{X_t} (kJ/mol)	A	r^2	ΔE_{X_t} (kJ/mol)	A	r^2
10	−20.976	−21.634	0.989	−16.914	−17.542	0.989
20	−17.929	−18.383	0.994	−16.138	−16.477	0.984
30	−16.923	−17.243	0.994	−16.835	−17.096	0.991
40	−16.708	−16.973	0.994	−16.615	−16.824	0.989
50	−16.813	−17.115	0.994	−17.090	−17.361	0.991
60	−17.509	−17.982	0.944	−17.354	−17.734	0.988
70	−18.198	−18.969	0.991	−19.114	−19.968	0.986
80	−25.034	−26.915	0.991	−26.643	−28.781	0.977
90	−24.990	−24.612	0.993	−73.457	−82.708	0.933

lowed by 30/70 and 40/60 blends. 50/50 and 75/25 blends present the lowest values of ΔE_{X_t} of sPP. Since the activation energy for crystallization of neat sPP is higher compared to its activation energy in the different blends, it suggests that iPP may play a role of nucleating agent towards sPP. However, there are two points corresponding to the 30/70 blend at 50% crystallinity and the 40/60 blend at 40% crystallinity that exhibit very high values of ΔE_{X_t}. Repeatability of these results has been verified. These results are not clear for us but our suggestion is that these drops of energy are probably due to some conformations that sPP chains might adopt during crystallization.

4.6. Evaluation of Hoffman–Lauritzen parameters U and K_g

ΔE_{X_t} dependence on X_t obtained from Friedman analysis is converted into ΔE dependence on T by replacing X_t with an average temperature T. This average temperature is determined using the $X_t = f(T)$ curves and by calculating the average T value for a specific X_t over the cooling rates range. In fact a specific X_t value is reached at different temperatures depending on the cooling rate used. Then the data obtained is fitted to Eq. (8) to evaluate U and K_g. Figs. 16 and 17 present ΔE as a function of temperature for iPP and sPP in each blend respectively. Solid lines represent fits of Eq. (8).

There is a decrease of ΔE with increasing temperature for iPP crystallization in neat iPP, 75/25 and 50/50 blends in most part of the temperature range investigated. Therefore, crystallization seems to become more difficult as temperature decreases. ΔE stops decreasing around 391 K and it constitutes a breakpoint corresponding to a change in crystallization regime. On the contrary, ΔE for iPP crystallization in 40/60 and 30/70 presents a more complex variation with many breakpoints over the temperature

Table 16
Effective energy barrier for non-isothermal crystallization of sPP for neat material and for iPP/sPP blends according to the differential iso-conversional method of Friedman.

$X(T)$ (%)	Neat sPP			75/25			50/50		
	ΔE_{X_t} (kJ/mol)	A	r^2	ΔE_{X_t} (kJ/mol)	A	r^2	ΔE_{X_t} (kJ/mol)	A	r^2
10	−3.717	−1.823	0.986	−9.285	−8.869	0.997	−8.985	−7.883	0.944
20	−3.335	−1.014	0.960	−9.137	−8.349	0.993	−8.223	−6.883	0.969
30	−2.966	0.388	0.949	−8.293	−7.235	0.996	−8.0122	−6.049	0.983
40	−2.665	0.031	0.939	−8.044	−6.892	0.996	−7.892	−6.535	0.994
50	−2.385	0.378	0.929	−7.914	−6.906	0.994	−8.381	−7.429	0.999
60	−2.172	0.562	0.934	−7.894	−8.357	0.991	−8.872	−8,844	0.999
70	−2.128	0.406	0.96	−8.236	−8.135	0.998	−10.578	−11.393	0.997
80	−2.173	0.009	0.98	−8.523	−9.202	0.986	−14.533	−18.138	0.975
90	−2.157	0.506	0.975	−9.044	−11.046	0.991	−10.512	−16.394	0.903

$X(T)$ (%)	40/60			30/70		
	ΔE_{X_t} (kJ/mol)	A	r^2	ΔE_{X_t} (kJ/mol)	A	r^2
10	−8.777	−12.238	0.978	−7.500	−10.475	0.942
20	−8.515	−11.728	0.987	−7.176	−9.826	0.959
30	−8.388	−11.559	0.992	−7.072	−9.660	0.972
40	−3.164	−11.342	0.995	−6.996	−9.627	0.976
50	−7.764	−10.935	0.995	−6.664	−9.297	0.969
60	−7.641	−11.039	0.996	−6.557	−9.388	0.964
70	−7.511	−11.231	0.991	−6.403	−9.528	0.955
80	−7.162	−11.283	0.954	−6.285	−9.907	0.938
90	−7.730	−13.168	0.963	−6.38	−10.995	0.940

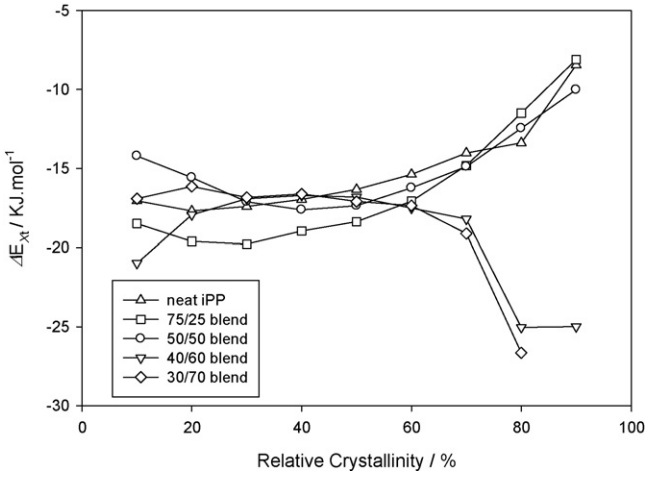

Fig. 14. Evolution of ΔE_{X_t} of iPP for the different materials as a function of relative crystallinity.

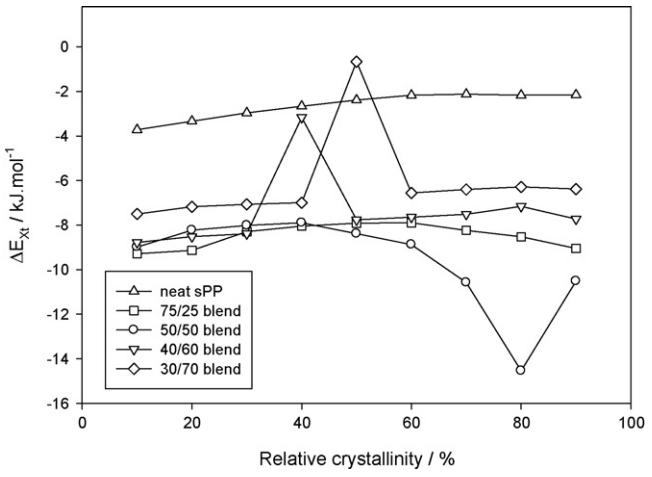

Fig. 15. Evolution of ΔE_{X_t} of sPP for the different materials as a function of relative crystallinity.

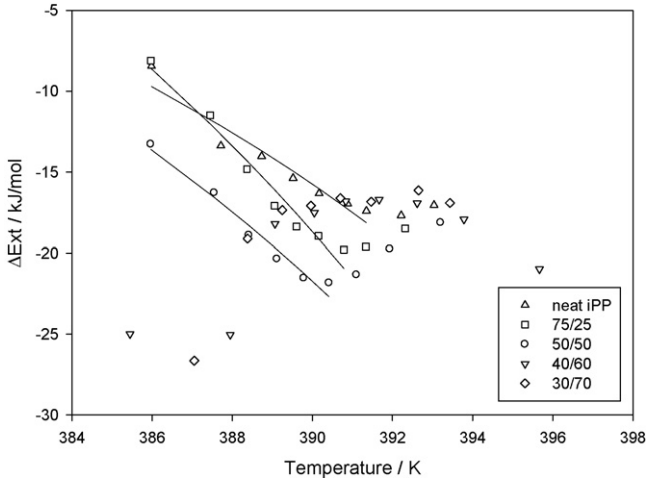

Fig. 16. Effective activation energy ΔE as a function of temperature of iPP for neat iPP and iPP/sPP blends. Solid lines represent fits of Eq. (8).

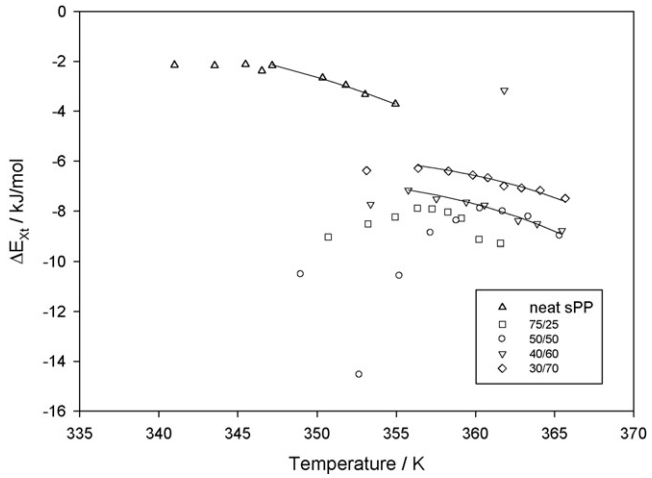

Fig. 17. Effective activation energy ΔE as a function of temperature of sPP for neat sPP and iPP/sPP blends. Solid lines represent fits of Eq. (8).

Table 17
Crystallization parameters of Hoffman–Lauritzen of iPP for neat iPP, 75/25 and 50/50 blends.

	U (kJ/mol)	$K_g \times 10^{-4}$ (K^2)	r^2	F_{stat}
Neat iPP	2.17	2.2	0.9270	63.5
75/25	4.15	3.6	0.9666	144.8
50/50	2.83	2.9	0.9696	127.9

range studied. There were not enough points between two successive breakpoints so that it was impossible to obtain reliable fits of Eq. (8) for these blends as shown in Fig. 16. There is also a decrease of ΔE with increasing temperature for sPP crystallization in neat sPP, 40/60 and 30/70 blends whereas variation for 50/50 and 75/25 blends are more complex. Because there were not enough points between two successive breakpoints in 50/50 and 75/25 blends, fits of Eq. (8) could only be performed for sPP in neat sPP, 40/60 and 30/70 blends as shown in Fig. 17. Results obtained from the fit of the data to Eq. (8) are reported in Tables 17 and 18.

U parameter is at least 10 times higher for iPP in neat iPP and 75/25 and 50/50 blends than for sPP in neat sPP and 40/60 and 30/70 blends. The same difference is observed between K_g values for iPP and K_g values for sPP. This difference confirms that crystallization rate is higher for iPP than for sPP as it has been observed from $X_t = f(t)$ curves. Moreover, these differences are probably linked to the difference of ΔE values between iPP in the various blends and sPP in the various blends (see Figs. 16 and 17).

K_g parameter for neat iPP is lower than K_g for iPP in 75/25 and 50/50 blends. It suggests a lower crystallization rate for neat iPP in neat iPP compared with iPP in 75/25 and 50/50 blends. However, K_g is higher for sPP in neat sPP than for sPP in 40/60 and 30/70 blends. It seems to be contradictory to the result shown on $X_t = f(t)$ curves. However we have to consider that the fit has been performed only on higher temperature portion of ΔE of neat sPP instead of the whole temperature range for 30/70 and 40/60 blends (there were

Table 18
Effective Crystallization parameters of Hoffman–Lauritzen of sPP for neat sPP, 40/60 and 30/70 blends.

	U (kJ/mol)	$K_g \times 10^{-4}$ (K^2)	r^2	F_{stat}
Neat sPP	8.2×10^{-2}	0.42	0.9936	401.4
40/60	2.9×10^{-1}	0.22	0.9524	119.9
30/70	3.3×10^{-1}	0.27	0.9651	1238.3

not enough points to perform a reliable fit of Eq. (8) on lower temperature portion of ΔE of neat sPP). Therefore K_g measured for neat sPP represents the crystallization rate of sPP only at higher temperatures. K_g for neat sPP in the whole temperature range may be lower because the decrease of ΔE occurs only in the higher temperature range.

F_{stat} and r^2 coefficients are satisfactory enough for us to consider that the fit of Eq. (8) is acceptable for the blends investigated.

5. Discussion

In this study, non-isothermal crystallization kinetics of iPP/sPP blends was investigated through DSC measurements. This study revealed that for low cooling rates iPP crystallizes a bit faster than sPP in many iPP/sPP blends and in neat materials. However this difference is attenuated when cooling rate is increased suggesting that cooling rate has a greater influence over sPP crystallization than iPP crystallization. Moreover t_{100} of both iPP and sPP is lower for iPP/sPP blends than for neat materials. These results could be explained by the fact that blending iPP or sPP with another component increases stress compared to neat material and promotes formation of crystallisation defaults that could act as nucleating sites. It is supported by the observation that for each cooling rate t_{100} of sPP is minimal in the 75/25 blend. In the 75/25 blend sPP constitutes the dispersed phase and therefore it suggests that when sPP is in the dispersed phase t_{100} is significantly decreased. Once again this can be due to the high level of stress that the component in the dispersed phase should be submitted to. This effect is not clearly evidenced for iPP in the 30/70 blend but it can be though anyway that iPP is subjected to such phenomenon when it is in the dispersed phase of an iPP/sPP blend (which is the case in the 30/70 blend). Finally, it is noteworthy that 50/50 blend do not always show results in accordance with the tendencies explained above and the reason may be its original co-continuous morphology which should generate unique properties.

Then, crystallization mechanisms taking place in iPP/sPP blends were studied through three different models which are Avrami model, Ozawa model and Mo model, using crystallization kinetics data from DSC measurements. According to Avrami, the main process taking place for iPP crystallization in iPP/sPP blends and in neat iPP is a nucleation followed by a spherulitic-like growth. However n_A decreases slightly for blends where iPP is in the dispersed phase so that the mechanism of crystal growth becomes half spherulitic and half disc-like. On the contrary sPP crystallizes mainly with a disc-like crystal growth whatever the blend composition is, as n_A lies mostly between 2 and 3.

Ozawa model shows some slight differences compared to Avrami. According to Ozawa, the spherulitic crystal growth for iPP takes place only in neat iPP and in the 75/25 blend. By increasing sPP content, the dimensionality of iPP crystallization decreases rapidly so that in the 40/60 and the 30/70 blend where iPP is in the dispersed phase the crystal growth is between disc-like and fibril like. Concerning sPP, the crystal growth is mainly fibril-like in iPP/sPP blends, due to n_O values between 1 and 2 and disc-like in neat sPP ($2 < n_O < 3$).

Ozawa and Avrami models display different results although the evolution of n_A and n_O with the blend composition is quite similar. Actually, n_A and n_O values for iPP decrease when iPP is in the dispersed phase. There is the same evolution for sPP with the composition of the blend as a decrease of n_A and n_O values in the blends compared to neat sPP is observed. As it was mentioned in introduction this decrease of n_A and n_O is linked with a decrease in the dimensionality of crystallites. An explanation of this decrease of the dimensionality of the crystal growth is that the dispersed phase is probably submitted to more stress than the continuous matrix. This increasing stress should hinders a crystal growth in the three directions and deform the crystallites, increasing by the way the number of defects in the crystallites. Consequently the deformation of crystallites should involve a decrease of n_A and n_O values compared to their values in neat materials where iPP and sPP are thought to be exposed to lower stress.

Crystallization rate constants K_A and K_O presented the same evolution as a function of cooling rate. However there are some differences concerning their values in neat iPP and sPP and in iPP/sPP blends. K_A values for neat iPP and sPP presented lower values compared to iPP/sPP blends whereas K_O values were higher for neat iPP and sPP compared with iPP/sPP blends. However r^2 fit coefficient and F coefficient indicate that K_A should be the most appropriate coefficient to describe iPP/sPP blends crystallization. Moreover, lower K_A values for neat iPP and sPP is the most probable hypothesis since blending iPP with sPP should induce stress and formation of defects that act as nucleation sites, which should raise the crystallization rate.

However, n_O values are found to be lower than n_A values for both iPP and sPP. This indicates that according to Ozawa model the crystal growth of both iPP and sPP in iPP/sPP blends is more constrained than it is when predicted by Avrami model. This difference has been confirmed by the analysis based upon Mo model showing that the n_A/n_O ratio exhibits some slight variation from 1. The highest variations from 1 for both iPP and sPP are observed for the 50/50 blend and the main reason is probably linked to the original co-continuous morphology of this blend. In the other materials a is mainly higher than 1, confirming the conclusion established by comparing both Avrami and Ozawa models that n_A is higher than n_O. However, iPP in 30/70 blend presents values of n_A/n_O which are lower than 1. As a consequence, it suggests the presence of some disagreements between the three models investigated and that they are not equally adapted to the iPP/sPP blends crystallization analysis.

Unfortunately, the r^2 fit coefficients are very high for both Ozawa, Avrami and Mo models and it is therefore difficult to draw any conclusions from these r^2 values. On the contrary, the determination of F_{stat} coefficient measuring the statistical reliability of the fit is very helpful to compare the methods. The highest values of F_{stat} are observed for Avrami model whereas Ozawa model shows very low values of F_{stat}. Those lower values of F_{stat} for Ozawa model clearly shows that this model is less adapted than Avrami model for the description of iPP/sPP blends crystallization. Some authors have reported such inefficiency of Ozawa model to describe crystallization of some semi-crystalline polymers mainly due to the occurrence of secondary crystallization on the later stages [30,45]. This is probably the reason here since a lowering of the trend of the $X_T(t)$ curves, corresponding to a secondary crystallization process, has been observed in the later stage of crystallization.

Determination of effective activation energy ΔE_{X_t} for sPP crystallization with the iso conversional method of Friedman showed that the energy barrier is higher when sPP is pure and when it is in the matrix of the blend than when sPP is in the dispersed phase. The most likely hypothesis is that when sPP is in the dispersed phase it is submitted to more stress than in the matrix and it may induce some inhomogeneities that could act as nucleation sites. It would therefore help sPP crystallization by reducing the energy barrier that has to be overcome. Moreover, the higher values of ΔE_{X_t} for neat sPP compared to values of ΔE_{X_t} for sPP in iPP/sPP blends could be explained by a nucleating effect of iPP towards sPP that has already been mentioned elsewhere [11,16,18]. This effect is less pronounced for iPP crystallization since values of ΔE_{X_t} are very close from one blend composition to another until 60% of relative crystallinity. This

is probably due to the fact that iPP crystallization is naturally more promoted than sPP crystallization as we have seen with Friedman method and therefore the impact of stress applied and additional nucleation sites on iPP is less significant. Beyond 60% of relative crystallinity, the same tendencies as these found for sPP are clearly observed.

ΔE_{X_t} evolution as a function of relative crystallinity determined with the Friedman method was converted into a variation of ΔE as a function of temperature. This data was fitted to the equation found by Hoffman–Lauritzen in order to evaluate U and K_g coefficients. The variations of ΔE for iPP in 40/60 and 30/70 blends were complex and therefore fit of Eq. (8) could not be performed. The complex variations may be due to the fact that iPP is in the dispersed phase in 40/60 and 30/70 blends and iPP should be submitted to a lot of stress. This stress may induce many changes in conformations and in crystallization regimes. The same tendencies were observed for sPP in 50/50 and 75/25 blends probably for the same reasons. Consequently, fits of Eq. (8) for sPP in 75/25 and 50/50 blends could not be performed too. U and K_g were found about 10 times higher for iPP in neat iPP and iPP/sPP blends than for sPP in neat sPP and iPP/sPP blends. It confirms that iPP crystallization rate is higher than sPP crystallization rate. K_g was found to be lower in neat iPP than in 75/25 and 50/50 blends. It indicates that iPP crystallization rate is higher in 75/25 and 50/50 blend than in neat iPP. This can be explained by the fact that blending iPP with sPP induces some stress and formation of defects and inhomogeneities that may have a nucleating effect. On the contrary, K_g for sPP in neat sPP is higher than K_g for sPP in 40/60 and 30/70 blends. However, K_g for sPP has been measured only in higher temperature range whereas K_g for sPP in 40/60 and 30/70 blends has been calculated over the entire temperature range investigated. Therefore it is difficult to compare K_g values and to draw any conclusions from this result. U parameter was found between 0.082 kJ mol^{-1} and 0.32 kJ mol^{-1} for sPP and between 2.17 kJ mol^{-1} and 4.15 kJ mol^{-1} for iPP. Although U is usually set to a universal value which lies at 6.3 kJ mol^{-1}, Hoffman et al. [40] showed that the best fit values lay between 4.2 kJ mol^{-1} and 16.7 kJ mol^{-1}. However, the values found for iPP are a bit lower than the values predicted by Hoffman and U values for sPP are much lower. This difference can be explained by the fact that the ΔE values involved in our study of iPP/sPP blends crystallization are very low and the variations of effective activation energies relative to crystallization extent and relative to temperature do not occur over a wide energy range. This is particularly true for sPP. Therefore it may be uneasy to have U values lying between 4.2 kJ mol^{-1} and 16.7 kJ mol^{-1} because these values have been obtained for materials in which greater effective activation energies variations were involved.

6. Conclusions

In this study, crystallization kinetics of iPP/sPP blends has been investigated through non-isothermal DSC analysis. DSC data shows that iPP and sPP crystallize separately in iPP/sPP blends and that sPP presents a double melting endotherm. Non-isothermal crystallization kinetics was analysed using Avrami model, Ozawa model and Mo model successively. Effective activation energies have been determined with Friedman method and the Hoffman–Lauritzen parameters were determined. Avrami, Ozawa and Mo models show similar tendencies but Avrami model seems to be the most accurate analysis. According to Avrami analysis, spherulitic growth is the main process talking place in iPP crystallization whatever the blend composition is. However, there are some parts of iPP in 40/60 and 30/70 blends which are forced to present a disc like crystallization due to the increasing stress as iPP goes from the matrix to the dispersed phase. On the other hand, growth of sPP crystallites in iPP/sPP blends is mainly disc-like during sPP crystallization with partial fibril-like growth. Moreover the variation of relative crystallinity of both iPP and sPP as a function of time and the determination of Hoffman–Lauritzen coefficients confirm that sPP crystallizes at a slower rate than iPP does. However, this difference can be attenuated by increasing cooling rate until times required for both iPP and sPP to achieve 100% of relative crystallinity become almost identical. This could be a very useful way to reduce stress inhomogeneities during processing steps like melt spinning and therefore to produce iPP/sPP fibres with new compositions and improved mechanical properties. Consequently, melt spinning of our iPP/sPP blends was attempted and analyses of mechanical properties of resulting fibres are still in progress in our laboratory.

Acknowledgements

The present work was part of the MEMOTI project which was financially supported by the Ministère de l'Economie, de l'Industrie et de l'Emploi and in particular the Direction Générale des Entreprises.

References

[1] G. Natta, I. Pasquon, A. Zambelli, J. Am. Chem. Soc. 84 (1962) 1488.
[2] G. Natta, I. Pasquon, P. Corradini, M. Peraldo, M. Pegoraro, A. Zambelli, Rend. Acad. Naz. Lincei 28 (1960) 539.
[3] J.A. Ewen, R.L. Jones, A. Razavi, J.D. Ferrara, J. Am. Chem. Soc. 110 (1988) 6255.
[4] F. Auriemna, O.R. de Ballesteros, C. de Rosa, Macromolecules 37 (2004) 7724.
[5] L. Guadagno, C. D'aniello, C. Naddeo, V. Vittoria, Macromolecules 35 (2002) 3921.
[6] A.J. Lovinger, B. Lotz, D.D. Davis, M. Schumacher, Macromolecules 27 (1994) 6603.
[7] F. Auriemna, O.R. de Ballesteros, C. de Rosa, Macromolecules 34 (2001) 4485.
[8] L. Guadagno, C. Naddeo, M. Raimondo, A. Senatore, V. Vittoria, Cryst. Growth Des. 6–7 (2006) 1703.
[9] C. de Rosa, F. Auriemna, Prog. Polym. Sci. 31 (2006) 145.
[10] F. Auriemna, C. de Rosa, J. Am. Chem. Soc. 125 (2003) 13143.
[11] X. Zhang, Y. Zhao, Z. Wang, C. Zheng, X. Dong, Z. Su, P. Sun, D. Wang, C.C. Han, D. Xu, Polymer 46 (2006) 5956.
[12] P. Supaphol, J.E. Spruiell, J. Appl. Polym. Sci. 75 (2000) 44.
[13] P. Supaphol, P. Thanomkiat, R.A. Phillips, Polym. Test. 23 (2004) 881.
[14] P. Supaphol, J.E. Spruiell, Polymer 42 (2001) 699.
[15] G. Gorassi, V. Vittoria, P. Longo, J. Appl. Polym. Sci. 80 (2001) 539.
[16] R. Thomann, J. Kressler, S. Setz, C. Wang, R. Mülhaupt, Polymer 37 (1996) 2627.
[17] R. Thomann, J. Kressler, R. Mülhaupt, Polymer 37 (1996) 2635.
[18] X.X. Zou, W. Yang, G.Q. Zheng, B.H. Xie, M.B. Yang, J. Polym. Sci.: Part B: Polym. Phys. 45 (2007) 2948.
[19] M. Avrami, J. Chem. Phys. 7 (1939) 1103.
[20] M. Avrami, J. Chem. Phys. 8 (1940) 212.
[21] M. Avrami, J. Chem. Phys. 9 (1941) 177.
[22] G. Prasath Balamurugan, S.N. Maiti, J. Appl. Polym. Sci. 107 (2008) 2414.
[23] Q.X. Zhang, Z.H. Zhang, H.F. Zhang, Z.S. Mo, J. Polym. Sci.-Polym. Phys. 40 (2002) 1784.
[24] X. Liu, C. Li, Y. Xiao, D. Zhang, W. Zeng, J. Appl. Polym. Sci. 102 (2006) 2493.
[25] M. Run, Y. Wang, C. Yao, J. Gao, Thermochim. Acta 447 (2006) 13.
[26] U.R. Evans, Trans. Faraday Soc. 41 (1945) 365.
[27] T. Ozawa, Polymer 12 (1971) 150.
[28] Y. Long, R.A. Shanks, Z.H. Stachurski, Prog. Polym. Sci. 20 (1995) 651.
[29] M. Eder, A. Wlochowicz, Polymer 24 (1983) 1593.
[30] Z. Qiu, Z. Mo, H. Zhang, R. Sheng, C.S. Song, Macromol. Sci. Phys. 39 (2000) 378.
[31] S.Y. Liu, Y.Y. Yu, Y. Cui, H.F. Zhang, Z.S. Mo, J. Appl. Polym. Sci. 70 (1998) 2371.
[32] J. Cai, T. Li, Y. Han, Y. Zhuang, X. Zhang, J. Appl. Polym. Sci. 100 (2006) 1479.
[33] H.E. Kissinger, Anal. Chem. 11 (1957) 1702.
[34] S. Vyazovkin, J. Comput. Chem. 22 (1997) 178.
[35] S. Vyazovkin, Macromol. Rapid Commun. 23 (2002) 771.
[36] H. Friedman, J. Polym. Sci. C6 (1964/1965) 183.
[37] Z. Ziaee, P. Supaphol, Polym. Test. 25 (2006) 807.

[38] S. Vyazovkin, N. Sbirrazzuoli, Macromol. Rapid Commun. 25 (2004) 733.
[39] S. Vyazovkin, I. Dranca, Macromol. Chem. Phys. 207 (2006) 20.
[40] J.D. Hoffman, G.T. Davis, J.I. Lauritzen Jr., in: N.B. Hannay (Ed.), Treatise on Solid State Chemistry, vol. 3, Plenum, NY, 1976, p. 497.
[41] P. Supaphol, J.E. Spruiell, J.S. Lin, Polym. Int. 49 (2000) 1473.
[42] J. Rodriguez-Arnold, A. Zhang, S.Z.D. Cheng, A.J. Lovinger, E.T. Hsieh, P. Chu, et al., Polymer 35 (1994) 1884.
[43] P. Supaphol, J. Appl. Polym. Sci. 78 (2000) 338.
[44] G.Z. Yang, X. Chen, Y. Xu, C.Z. Li, P. Wu, T. Liu, Polym. Int. 56 (2007) 245.
[45] T.X. Liu, Z.S. Mo, H.F. Zhang, J. Polym. Eng. 18 (1998) 283.